Supplementary Material (ESI) for Journal of Materials Chemistry

Regulating Low-Dimensional Magnetic Behavior of Organic Radicals in Crystalline Hydrogen-Bonded Host Frameworks

*Airon C. Soegiarto, Wah Yan, Andrew D. Kent, and Michael D. Ward**

Contribution from Department of Physics, New York University, 4 Washington Place, New York, NY 10003, and Molecular Design Institute, Department of Chemistry, New York University, 100 Washington Square East, New York, NY 10003

Electronic Supplementary Information

Figure S1. EPR spectra of **G$_2$BPDS**·2(*TEMPO*), **G$_2$NDS**·2(*TEMPO*), **G$_2$ABDS**·½(*TEMPO*)·½(MeOH), **G$_2$BPDS**·2(*MeO-TEMPO*), **G$_2$ABDS**·½(*MeO-TEMPO*)·½(MeOH), and **G$_2$BPDS**·(*oxo-TEMPO*)·(MeOH)·(H$_2$O).

Figure S2. Effect of anisotropy in the EPR spectra of **G$_2$BPDS**·2(*TEMPO*), **G$_2$BPDS**·2(*MeO-TEMPO*), and **G$_2$ABDS**·½(*TEMPO*)·½(MeOH).

Figure S3. Plot of: (A) χ_{mol} *vs. T*; (B) $1/\chi_{mol}$ *vs. T*; (C) $\chi_{mol}T$ *vs. T* for **G$_2$ABDS**·½(*MeO-TEMPO*)·½(MeOH).

Figure S4. Plot of: (A) χ_{mol} *vs. T*; (B) $1/\chi_{mol}$ *vs. T*; (C) $\chi_{mol}T$ *vs. T* for **G$_2$BPDS**·2(*MeO-TEMPO*).

Figure S5. Plot of: (A) χ_{mol} *vs. T*; (B) $1/\chi_{mol}$ *vs. T*; (C) $\chi_{mol}T$ *vs. T* for **G$_2$BPDS**·(*oxo-TEMPO*)·(MeOH)·(H$_2$O).

Figure S6. Plot of: (A) χ_{mol} *vs. T*; (B) $1/\chi_{mol}$ *vs. T*; (C) $\chi_{mol}T$ *vs. T* for TEMPO.

Figure S7. Plot of: (A) χ_{mol} *vs. T*; (B) $1/\chi_{mol}$ *vs. T*; (C) $\chi_{mol}T$ *vs. T* for MeO-TEMPO.

Figure S8. Plot of: (A) χ_{mol} *vs. T*; (B) $1/\chi_{mol}$ *vs. T*; (C) $\chi_{mol}T$ *vs. T* for oxo-TEMPO.

Figure S9. The experimental χ_{mol} data of **G$_2$BPDS**·2(*TEMPO*) fitted with the 1-D chain Bonner-Fisher, Hatfield, and Pade models.

Figure S10. The experimental χ_{mol} data of **G$_2$NDS**·2(*TEMPO*) fitted with the 2-D square-planar model.

Figure S11. Plot of M_{molar} *vs. H* for **G$_2$ABDS**·½(*TEMPO*)·½(MeOH).

Figure S12. Plot of M_{molar} *vs. H* for **G$_2$ABDS**·½(*MeO-TEMPO*)·½(MeOH).

Figure S13. Plot of M_{molar} *vs. H* for **G$_2$BPDS**·2(*MeO-TEMPO*).

Figure S14. Plot of M_{molar} *vs. H* for **G$_2$BPDS**·(*oxo-TEMPO*)·(MeOH)·(H$_2$O).

Figure S15. Plot of M_{molar} *vs. H* for TEMPO.

Figure S16. Plot of M_{molar} *vs. H* for MeO-TEMPO.

Figure S17. Plot of M_{molar} *vs. H* for oxo-TEMPO.

CIF files

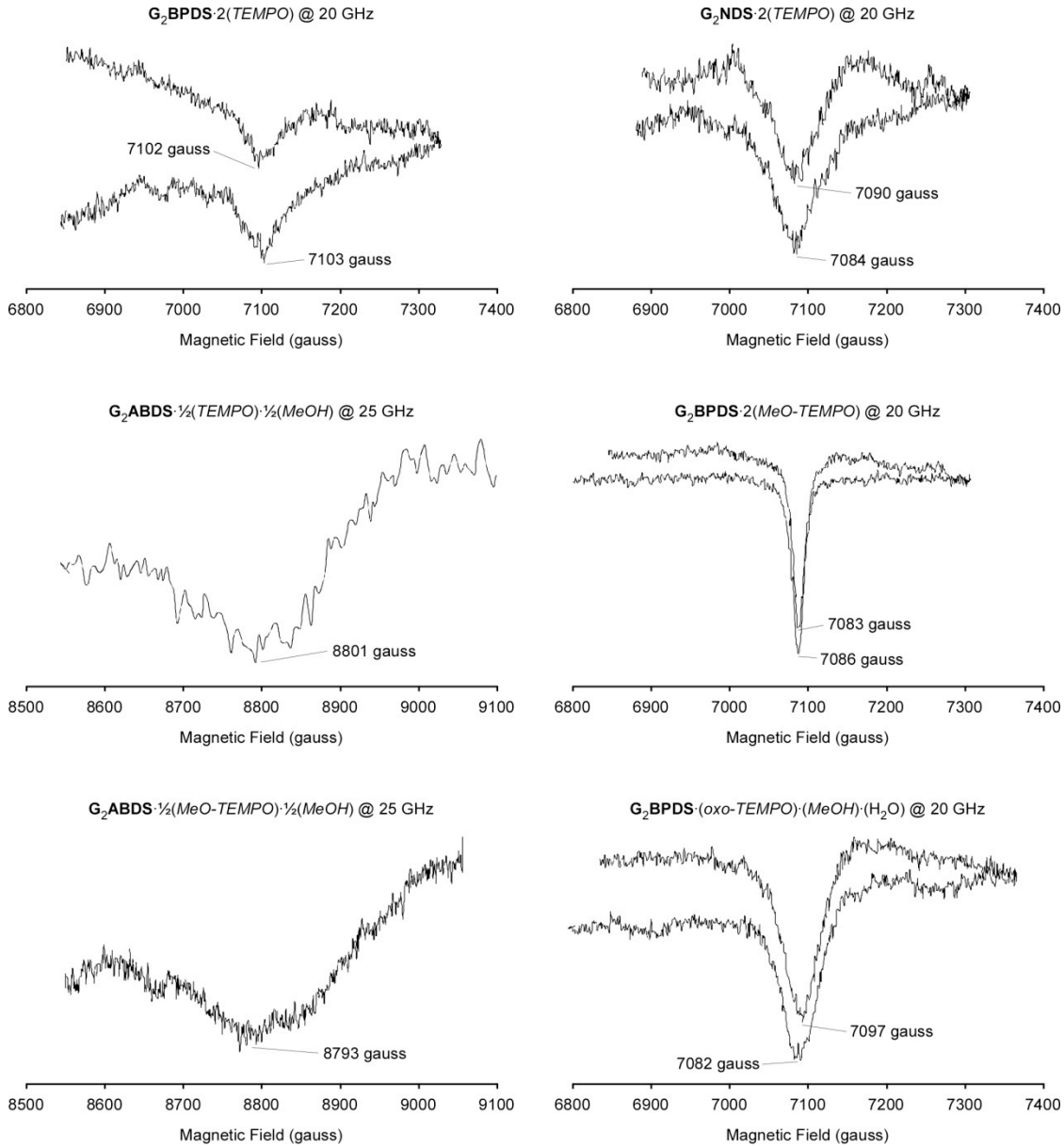

Figure S1. EPR spectra of the GDS inclusion compounds at room temperature. EPR experiments of **G**$_2$**BPDS**·2(*TEMPO*), **G**$_2$**NDS**·2(*TEMPO*), **G**$_2$**BPDS**·2(*MeO-TEMPO*), and **G**$_2$**BPDS**·(*oxo-TEMPO*)·(MeOH)·(H$_2$O) were performed in a 20 GHz field, whereas those of **G**$_2$**ABDS**·½(*TEMPO*)·½(MeOH) and **G**$_2$**ABDS**·½(*MeO-TEMPO*)·½(MeOH) were performed in a 25 GHz field due to a weaker magnetic response. The direction of the applied magnetic field (*H*) is parallel to the longest physical dimension of the crystals.

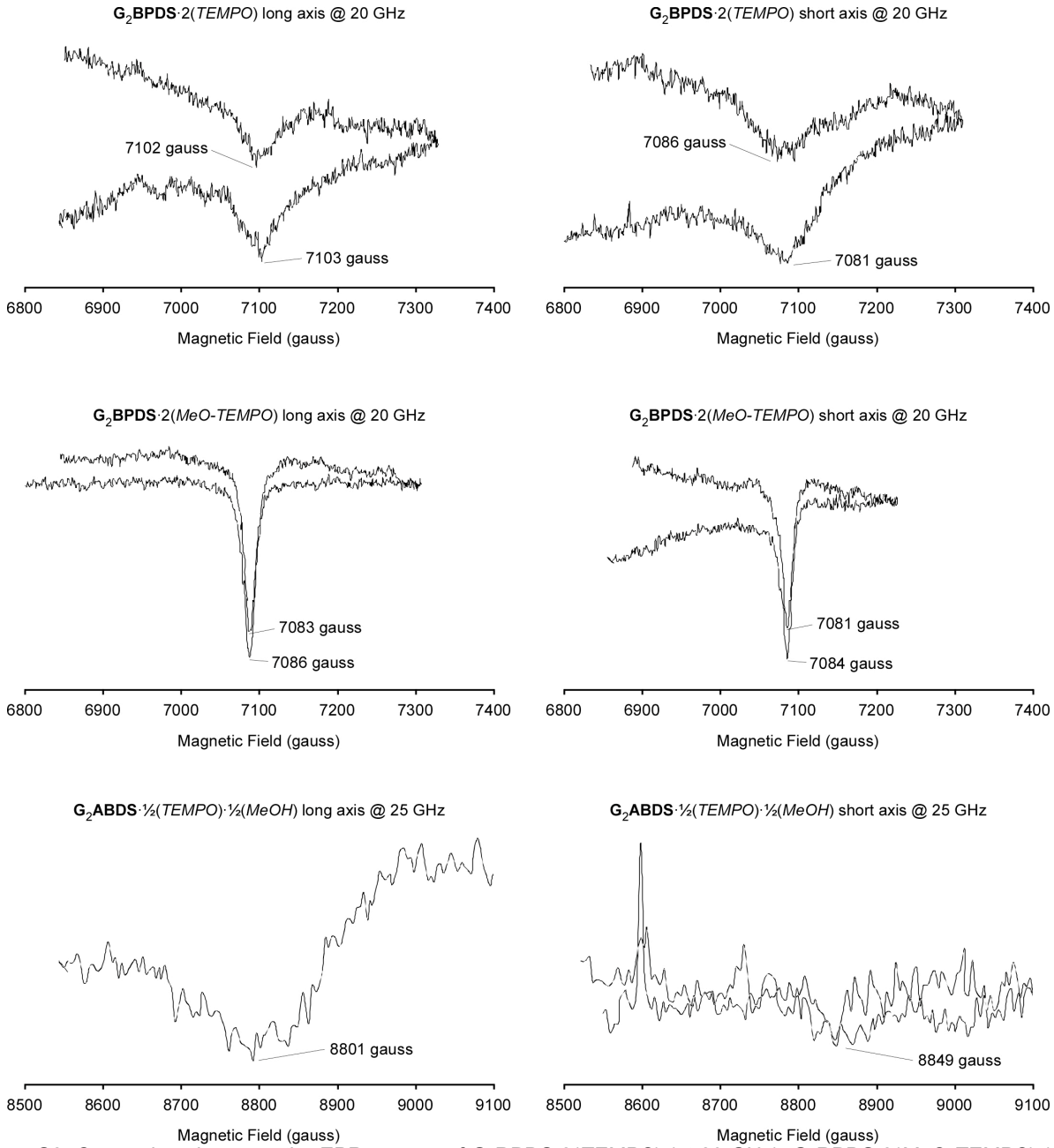

Figure S2. Comparison between the EPR spectra of **G$_2$BPDS**·2(*TEMPO*) (at 20 GHz), **G$_2$BPDS**·2(*MeO-TEMPO*) (at 20 GHz), and **G$_2$ABDS**·½(*TEMPO*)·½(MeOH) (at 25 GHz) taken with the applied magnetic field (*H*) parallel to the longest physical dimension of the crystals (on the left panel) and those taken with *H* perpendicular to the longest physical dimension of the crystals (on the right panel). In all cases, the difference in the calculated *g* value is less than 1%.

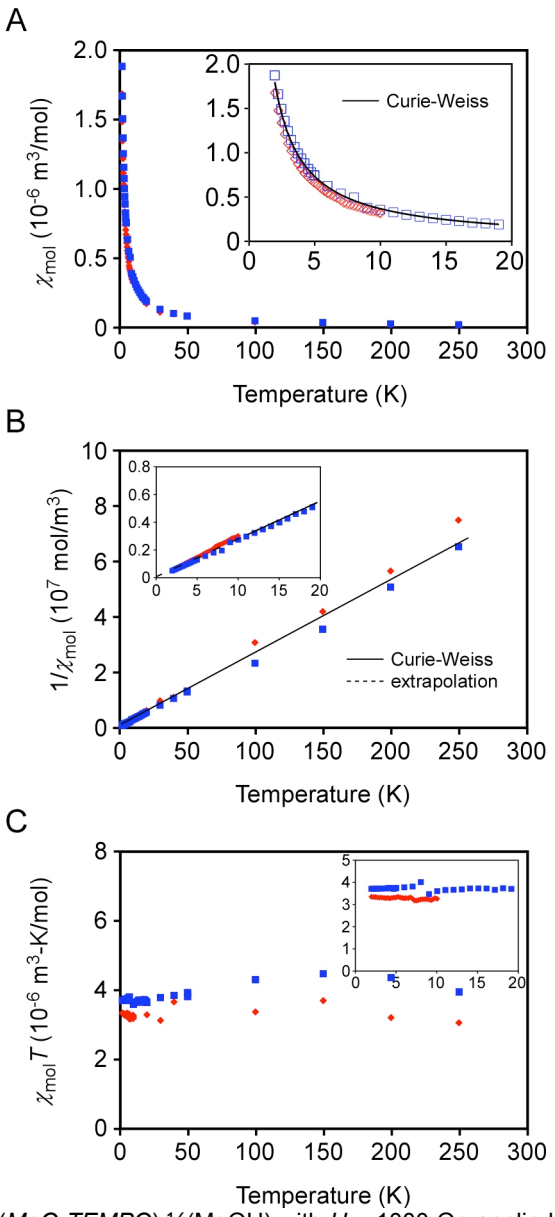

Figure S3. (A) χ_{mol} of **G$_2$ABDS**·½(*MeO-TEMPO*)·½(MeOH) with H = 1000 Oe applied parallel to the longest physical dimension of the crystal. The red data points (♦, ◊) are collected in a heating cycle from 2 K to 300 K, whereas the blue data points (■, □) are collected in a cooling cycle from 300 K to 2 K. The inset panel depicts a blowup between T = 2 K and 20 K and the Curie-Weiss (solid curve) fit to the data. (B) Dependence of $1/\chi_{mol}$ on temperature. The Curie-Weiss fit (solid line) and extrapolation to T = 0 K are shown in the inset. (C) Dependence of $\chi_{mol}T$ (analogous to μ_{eff}) on temperature. The susceptibility data have been corrected using Pascal's constants to account for the contribution from the diamagnetic components of the inclusion compound.

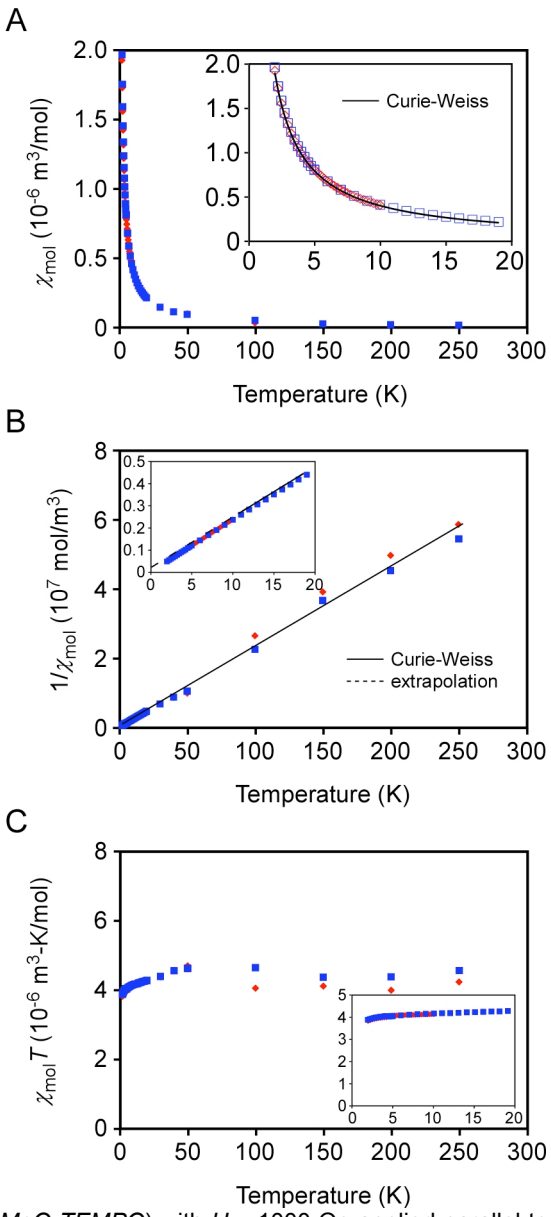

Figure S4. (A) χ_{mol} of **G**$_2$**BPDS**·2(*MeO-TEMPO*) with H = 1000 Oe applied parallel to the longest physical dimension of the crystal. The red data points (♦, ◊) are collected in a heating cycle from 2 K to 300 K, whereas the blue data points (■, □) are collected in a cooling cycle from 300 K to 2 K. The inset panel depicts a blowup between T = 2 K and 20 K and the Curie-Weiss (solid curve) fit to the data. (B) Dependence of $1/\chi_{mol}$ on temperature. The Curie-Weiss fit (solid line) and extrapolation to T = 0 K are shown in the inset. (C) Dependence of $\chi_{mol}T$ (analogous to μ_{eff}) on temperature. The susceptibility data have been corrected using Pascal's constants to account for the contribution from the diamagnetic components of the inclusion compound.

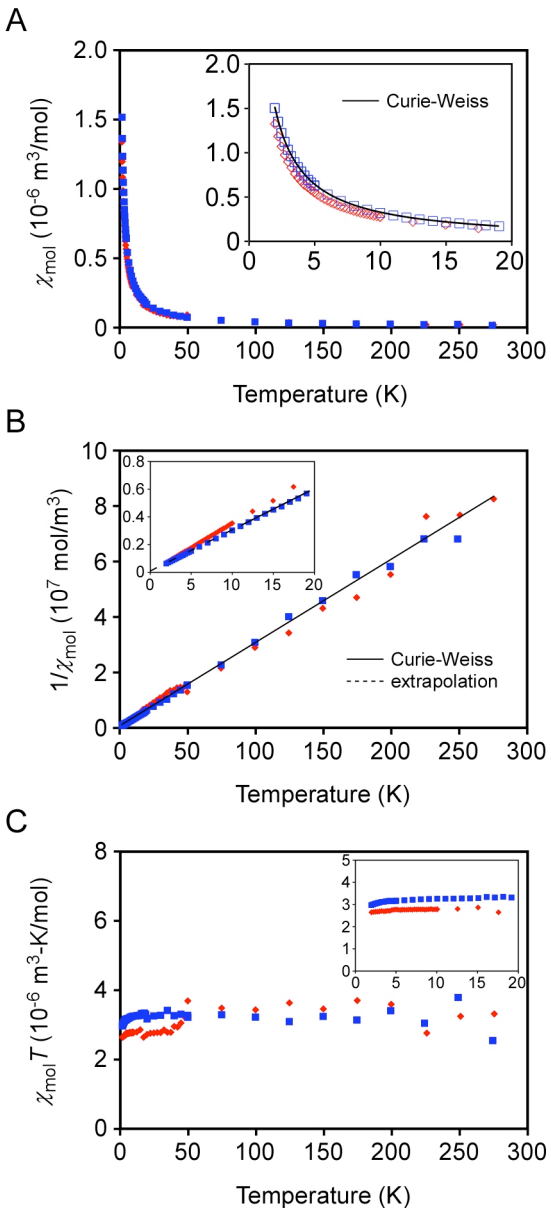

Figure S5. (A) χ_{mol} of **G$_2$BPDS**·(*oxo-TEMPO*)·(MeOH)·(H$_2$O) with H = 1000 Oe applied parallel to the longest physical dimension of the crystal. The red data points (♦, ◊) are collected in a heating cycle from 2 K to 300 K, whereas the blue data points (■, □) are collected in a cooling cycle from 300 K to 2 K. The inset panel depicts a blowup between T = 2 K and 20 K and the Curie-Weiss (solid curve) fit to the data. (B) Dependence of $1/\chi_{mol}$ on temperature. The Curie-Weiss fit (solid line) and extrapolation to T = 0 K are shown in the inset. (C) Dependence of $\chi_{mol}T$ (analogous to μ_{eff}) on temperature. The susceptibility data have been corrected using Pascal's constants to account for the contribution from the diamagnetic components of the inclusion compound.

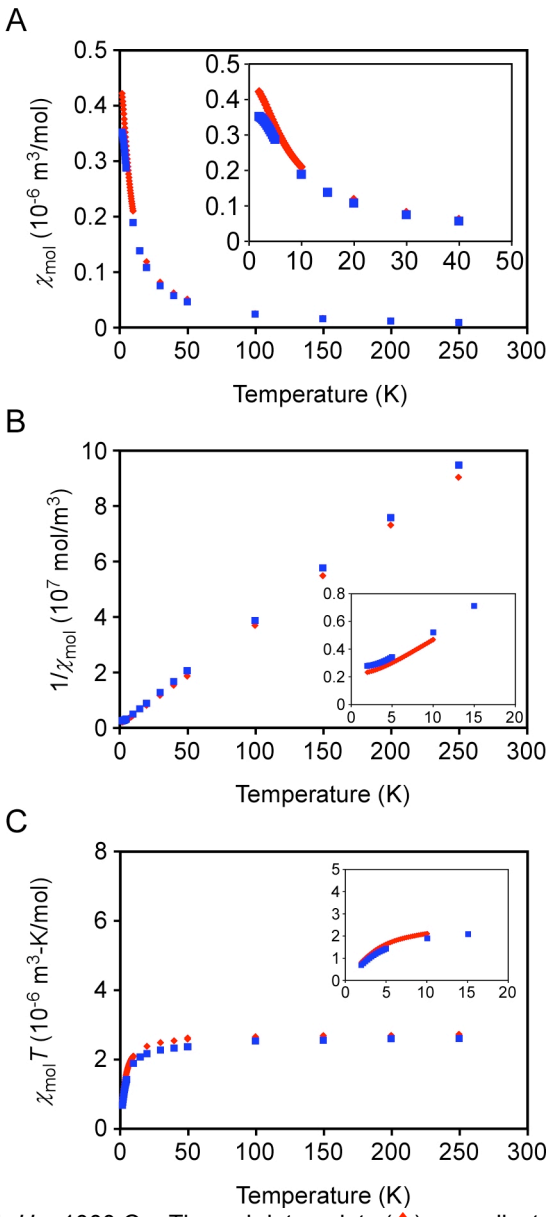

Figure S6. (A) χ_{mol} of TEMPO with H = 1000 Oe. The red data points (♦) are collected in a heating cycle from 2 K to 300 K, whereas the blue data points (■) are collected in a cooling cycle from 300 K to 2 K. The inset panel depicts a blowup between T = 2 K and 20 K. (B) Dependence of $1/\chi_{mol}$ on temperature. (C) Dependence of $\chi_{mol}T$ (analogous to μ_{eff}) on temperature. The susceptibility data have been corrected using Pascal's constants to account for the contribution from the diamagnetic components.

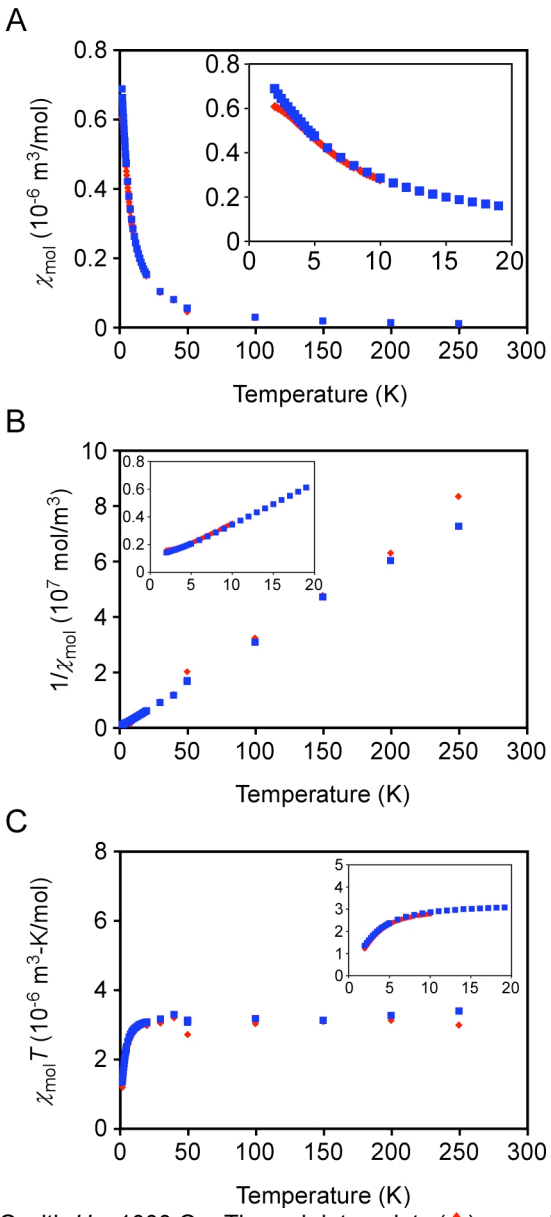

Figure S7. (A) χ_{mol} of MeO-TEMPO with H = 1000 Oe. The red data points (♦) are collected in a heating cycle from 2 K to 300 K, whereas the blue data points (■) are collected in a cooling cycle from 300 K to 2 K. The inset panel depicts a blowup between T = 2 K and 20 K. (B) Dependence of $1/\chi_{mol}$ on temperature. (C) Dependence of $\chi_{mol}T$ (analogous to μ_{eff}) on temperature. The susceptibility data have been corrected using Pascal's constants to account for the contribution from the diamagnetic components.

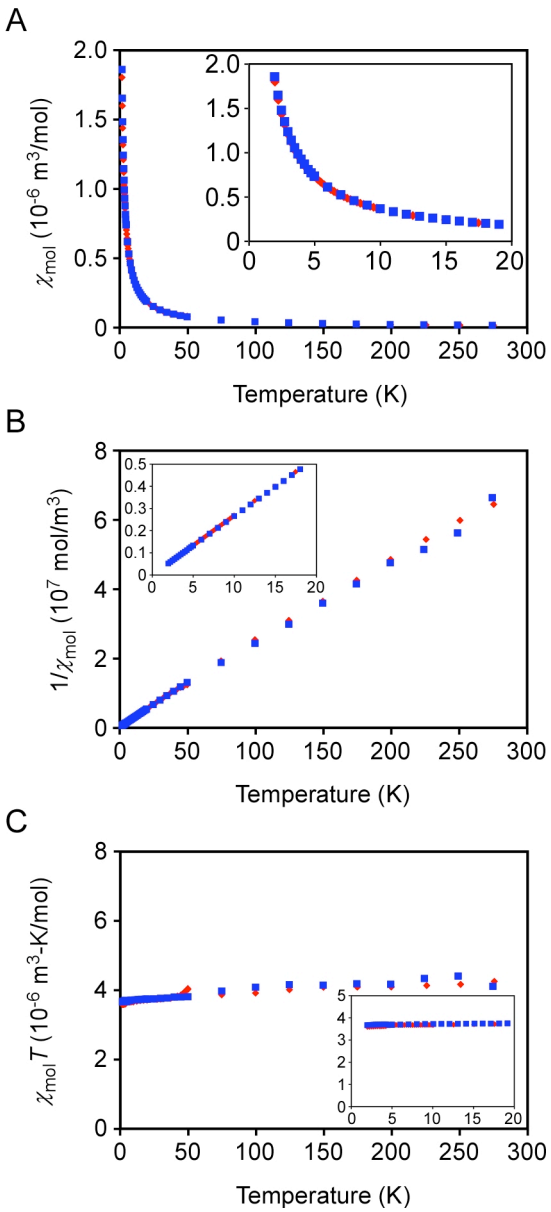

Figure S8. (A) χ_{mol} of oxo-TEMPO with H = 1000 Oe. The red data points (♦) are collected in a heating cycle from 2 K to 300 K, whereas the blue data points (■) are collected in a cooling cycle from 300 K to 2 K. The inset panel depicts a blowup between T = 2 K and 20 K. (B) Dependence of $1/\chi_{mol}$ on temperature. (C) Dependence of $\chi_{mol}T$ (analogous to μ_{eff}) on temperature. The susceptibility data have been corrected using Pascal's constants to account for the contribution from the diamagnetic components.

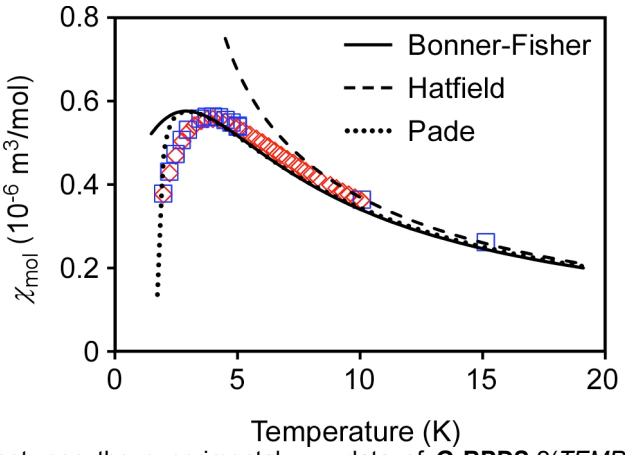

Figure S9. Poor correlation between the experimental χ_{mol} data of **G$_2$BPDS**·2(*TEMPO*) and the calculated χ_{mol} obtained from the 1-D chain Bonner-Fisher, Hatfield, and Pade models.

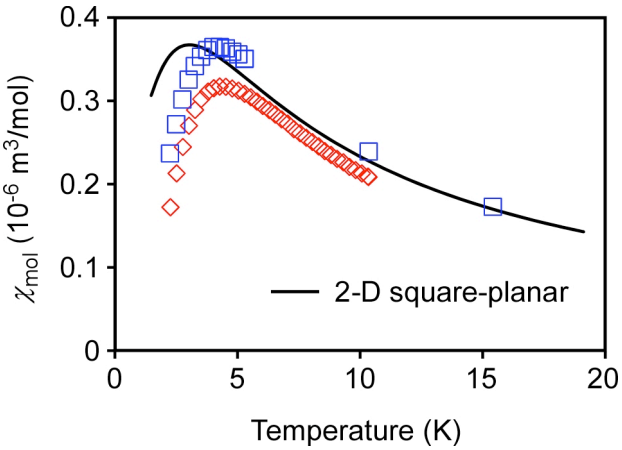

Figure S10. Poor correlation between the experimental χ_{mol} data of **G$_2$NDS**·2(*TEMPO*) and the calculated χ_{mol} obtained from the 2-D square-planar model.

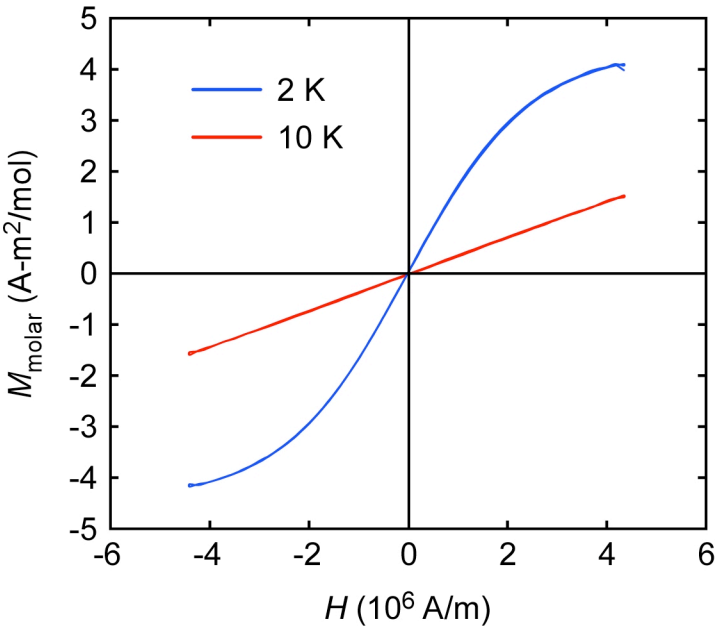

Figure S11. Dependence of M_{molar} on H at T = 2 K (blue line) and T = 10 K (red line) for **G**$_2$**ABDS**·½(*TEMPO*)·½(MeOH). Note that 1 Oe = 1000/4π A/m. The field H is applied parallel to the longest physical dimension of the crystal. The magnetization data have been corrected to account for the contribution from the diamagnetic components of the inclusion compounds.

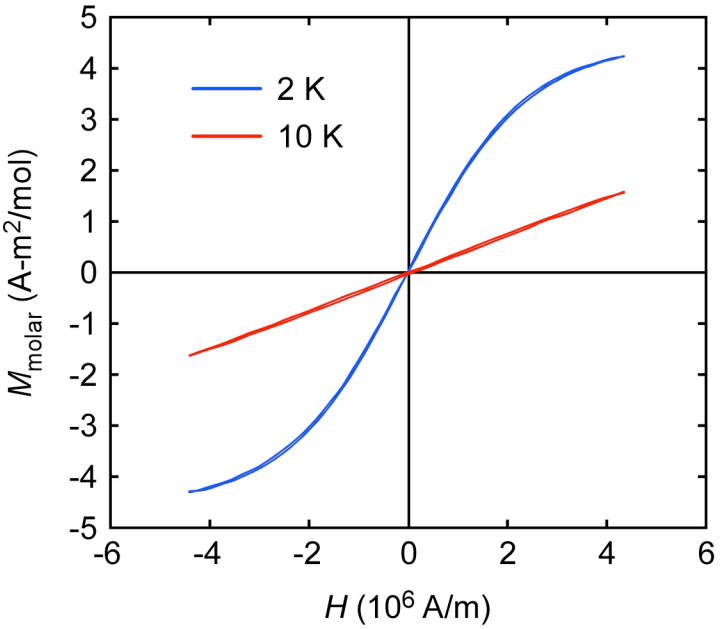

Figure S12. Dependence of M_{molar} on H at T = 2 K (blue line) and T = 10 K (red line) for **G**$_2$**ABDS**·½(*MeO-TEMPO*)·½(MeOH). Note that 1 Oe = 1000/4π A/m. The field H is applied parallel to the longest physical dimension of the crystal. The magnetization data have been corrected to account for the contribution from the diamagnetic components of the inclusion compounds.

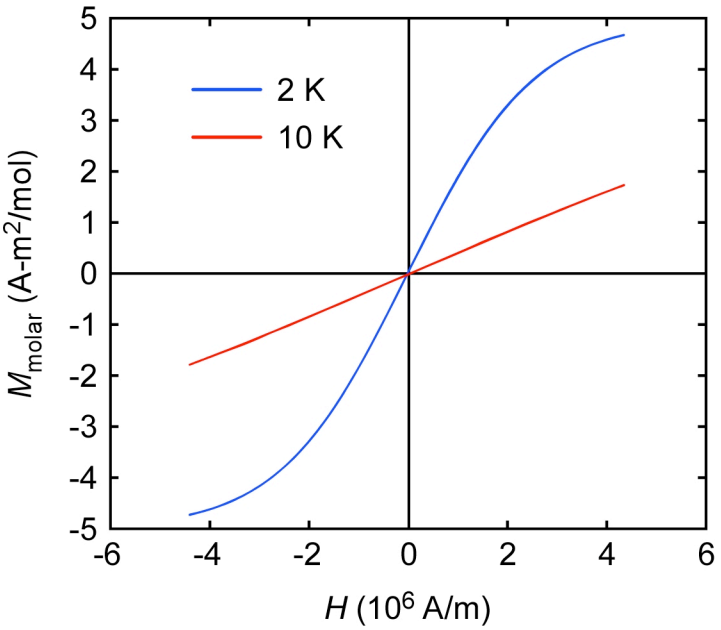

Figure S13. Dependence of M_{molar} on H at T = 2 K (blue line) and T = 10 K (red line) for **G**$_2$**BPDS**·2(*MeO-TEMPO*). Note that 1 Oe = 1000/4π A/m. The field H is applied parallel to the longest physical dimension of the crystal. The magnetization data have been corrected to account for the contribution from the diamagnetic components of the inclusion compounds.

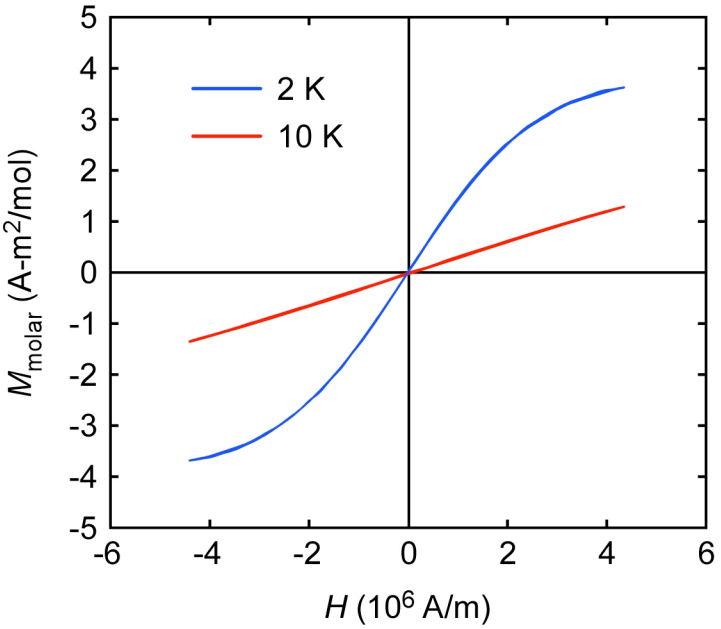

Figure S14. Dependence of M_{molar} on H at T = 2 K (blue line) and T = 10 K (red line) for **G**$_2$**BPDS**·(*oxo-TEMPO*)·(MeOH)·(H_2O). Note that 1 Oe = 1000/4π A/m. The field H is applied parallel to the longest physical dimension of the crystal. The magnetization data have been corrected to account for the contribution from the diamagnetic components of the inclusion compounds.

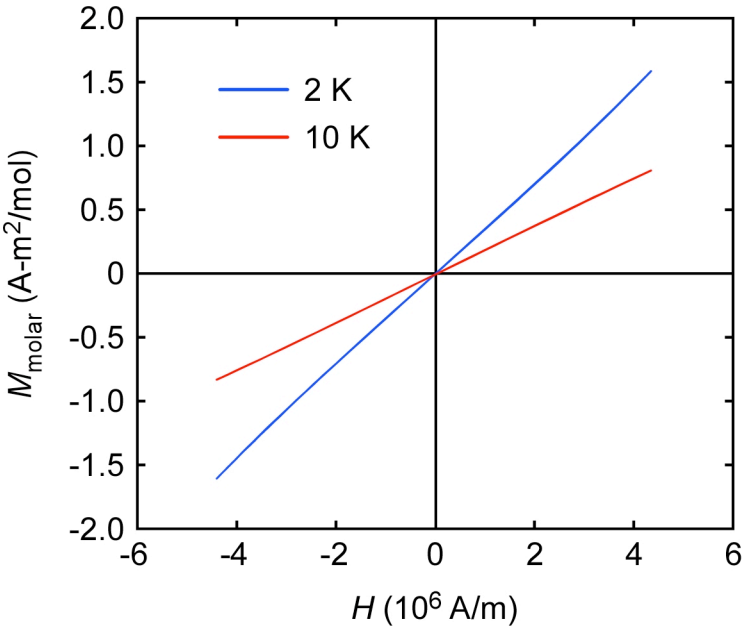

Figure S15. Dependence of M_{molar} on H at T = 2 K (blue line) and T = 10 K (red line) for TEMPO. Note that 1 Oe = 1000/4π A/m. The magnetization data have been corrected to account for the contribution from the diamagnetic components.

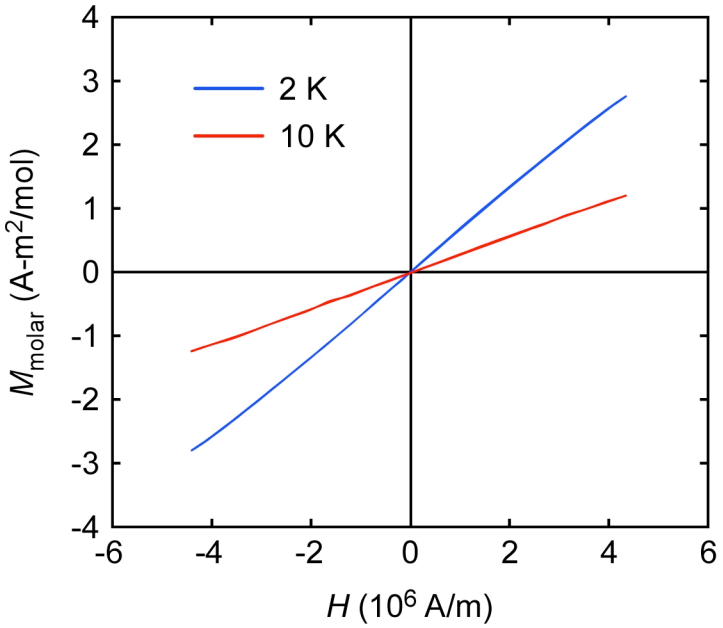

Figure S16. Dependence of M_{molar} on H at T = 2 K (blue line) and T = 10 K (red line) for MeO-TEMPO. Note that 1 Oe = 1000/4π A/m. The magnetization data have been corrected to account for the contribution from the diamagnetic components.

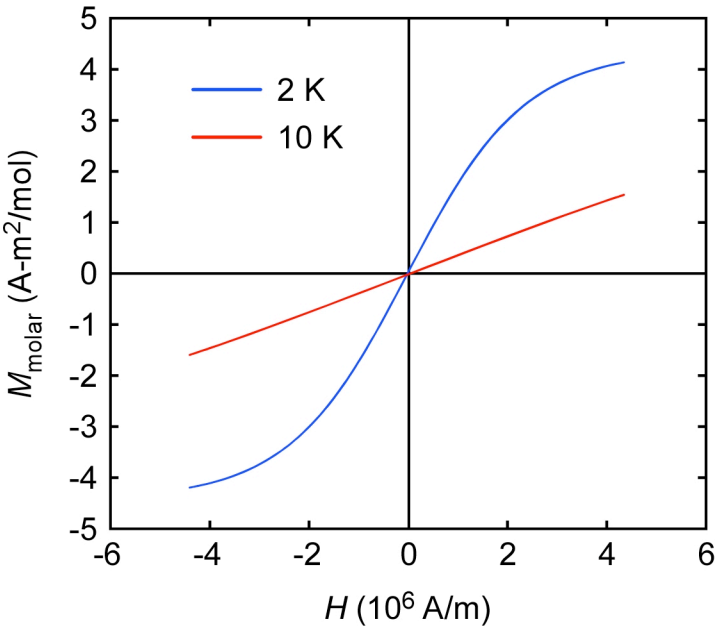

Figure S17. Dependence of M_{molar} on H at T = 2 K (blue line) and T = 10 K (red line) for oxo-TEMPO. Note that 1 Oe = 1000/4π A/m. The magnetization data have been corrected to account for the contribution from the diamagnetic components.

CIF files

G_2NDS·2(*TEMPO*) – GDS 1.cif

G_2BPDS·2(*TEMPO*) – GDS 2.cif

G_2ABDS·½(*TEMPO*)·½(MeOH) – GDS 3.cif

G_2SBDS·½(*TEMPO*)·½(MeOH) – GDS 4.cif

G_2BPDS·2(*MeO-TEMPO*) – GDS 5.cif

G_2ABDS·½(*MeO-TEMPO*)·½(MeOH) – GDS 6.cif

G_2BPDS·(*oxo-TEMPO*)·(MeOH)·(H_2O) – GDS 7.cif

G_2ABDS·(*oxo-TEMPO*)·(H_2O) – GDS 8.cif